Photogeneration and Migration of Electrons and Holes in Zeolite NaY

Melanie A. O'Neill, Frances L. Cozens,* and Norman P. Schepp

Department of Chemistry, Dalhousie University, Halifax, Nova Scotia, Canada, B3H 4J3

Received: July 26, 2001; In Final Form: October 16, 2001

Electron transfer and charge migration between electron donors and acceptors encapsulated within dry NaY zeolites are explored using nanosecond laser flash photolysis. The role of the zeolite in these redox processes is examined in order to characterize the intrazeolite mobility of electrons and holes. Electron migration is initiated by photoexciting *trans*-anethole in NaY containing coadsorbed 1,4-dicyanobenzene as an electron acceptor, while hole migration is initiated by photoexciting chloranil in NaY containing coadsorbed 4,4′-dimethoxybicumene as an electron donor. The experimental results demonstrate that ultrafast redox reactions ($>10^8$ s^{-1}) take place, leading to long-lived charge separated species within the zeolite cavities. The efficiency of these redox processes is examined as a function of donor−acceptor concentration and the presence of nitrous oxide as an electron trap. Interpretation of the experimental data with two independent models provides evidence that the redox chemistry occurring within NaY cannot be completely accounted for by contact interactions between the incorporated molecules. From these models, it is estimated that the zeolite can mediate electron and hole migration over vacant, through-space distances of 11 and 18 Å, respectively.

Introduction

Investigations of intrazeolite reaction dynamics continue to improve our understanding of host−guest interactions and the roles that zeolites play in photochemical and thermal transformations of guest molecules.[1−6] The ability of zeolites to host molecular guests in supramolecular assemblies and to catalyze chemical reactions is a consequence of the unique structural and physicochemical features of these materials. Zeolites[7−10] are crystalline aluminosilicates possessing an open framework of molecular-sized pores, channels, and cavities. Many molecules are readily adsorbed within this microporous network, and physical and chemical transformations can occur on the large internal surfaces. The regular periodic array of void spaces throughout the zeolite particle, typically 0.1 to 10 μm in length, facilitates the novel spatial arrangement of thousands of molecules with significant long-range ordering. In addition, the internal zeolite environment is characterized by a negatively charged lattice with interstitial charge-balancing cations residing within the micropores. These combined structural and chemical features generate a strongly polar anionic network of well-defined void spaces with localized electrostatic fields and active acidic and basic sites. Consequently, zeolites are very effective organized media for confining molecular guests and manipulating their reactivity, and zeolites have been heavily exploited commercially in a vast array of diverse applications,[11,12] most notably as heterogeneous catalysts for reactions in the petrochemical industry and the synthesis of fine chemicals.[13] The attractive and versatile properties of zeolites have also rendered these materials a favorite in academic research. A common theme in much of the current research is the application of the local environment within zeolites to control or manipulate reaction dynamics, and there has been considerable interest in the ability of these solid materials to modify and/or promote a variety of fundamental reactions in organic chemistry.[14−30]

The transfer of a single electron between two molecules is one of the most significant and ubiquitous reactions in the chemical and biological world, and electron transfer (ET) continues to be among the most actively pursued areas in contemporary chemistry.[31−33] Experimental attempts to emulate efficient photoinduced electron transfer (PET) in natural systems often employ organized, heterogeneous media[34,35] to modify ET dynamics, and research has been directed toward practical applications such as solar energy conversion,[36] photosynthetic mimicry,[37−39] and molecular electronics.[40,41] Such experiments probe ET reactions in novel environments, providing insight into the mechanisms of these reactions as well as the nature and influence of the media. Zeolites have proven to be highly amenable hosts in many studies of heterogeneous PET reactions between redox pairs co-included within the zeolite matrix, and/or at the zeolite interface.[6,20,25−27,29,39,42−57] To date, these investigations have revolved around three broad and somewhat interdependent themes: (*i*) decreasing the rate of back electron transfer (BET) through zeolite encapsulation; (*ii*) using zeolitic assemblies to achieve long-lived charge separation in PET reactions aimed at practical applications such as artificial photosynthesis; and (*iii*) employing the zeolite as a microscopic reactor to modify the dynamics of PET and the resultant products as compared to homogeneous media.

Results from these experimental investigations have generated considerable insight into the ability of zeolitic systems to modify PET reactions in useful ways. However, the mechanisms of ET reactions between donors and acceptors co-included within zeolites have not yet been extensively explored. This is especially true with regard to the possibility of long distance ET chemistry among molecules spatially separated within the zeolite matrix.[58,59]

The current investigation examines the generation and migration of electrons and holes within the channels and cavities of dry NaY. The electrons are generated by laser-induced photoionization of a zeolite encapsulated guest, *trans*-anethole (An). The holes are generated by a PET reaction between the zeolite and an encapsulated guest, chloranil (Chl), where the zeolite acts as an electron donor. The mobility of the resultant electrons and holes is probed by including a secondary electron acceptor,

* Corresponding author. E-mail: fcozens@is.dal.ca.

10.1021/jp015518j CCC: $20.00
Published on Web 11/30/2001

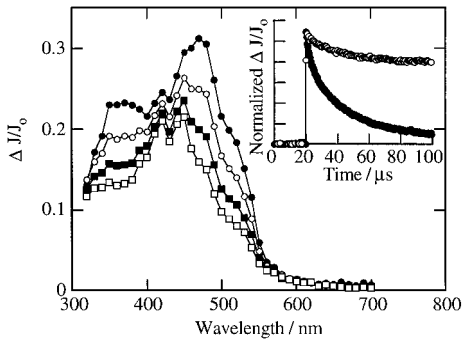

Figure 1. Transient diffuse reflectance spectrum obtained 480 ns (closed circles), 2.48 μs (open circles), 7.20 μs (closed squares), and 14.12 μs (open squares) after 308 nm laser photolysis of Chl ($\langle S\rangle$ = 0.08) in evacuated dry NaY. The inset shows the normalized decay traces monitored at 500 nm (closed circles) and 420 nm (open circles).

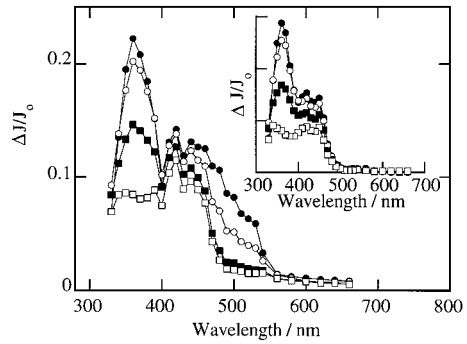

Figure 2. Transient diffuse reflectance spectrum obtained 400 ns (closed circles), 880 ns (open circles), 3.32 μs (closed squares), and 13.6 μs (open squares) after 308 nm laser photolysis of Chl ($\langle S\rangle$ = 0.04) in evacuated dry NaY containing coadsorbed DMB ($\langle S\rangle$ = 0.1). Inset shows the transient diffuse reflectance spectrum observed at the same time delays following 308 nm laser irradiation of the same sample in the presence of oxygen.

1,4-dicyanobenzene (DCB), or electron donor, 4,4′-dimethoxybicumene (DMB), within the framework to scavenge the electron or hole, thereby generating a spectroscopically visible intermediate. Each of these processes occurs rapidly within the nanosecond laser pulse. The yields of electron or hole migration and trapping are determined from the spectroscopic measurements and interpreted using two independent models, the Perrin model and the distribution model, to estimate the distances that electrons and holes may travel within the zeolite matrix.

Results

Nanosecond Laser Flash Photolysis of Chloranil in NaY. The transient diffuse reflectance spectrum observed immediately following 308 nm laser excitation of Chl included in evacuated (10^{-4} Torr) dry NaY is dominated by intense absorption between 320 and 550 nm, Figure 1. Absorption by at least two different transient species is clearly evident by the distinctly different decays observed within the spectrum. For instance, at wavelengths greater than about 480 nm and less than 400 nm, the transient decay is significantly more rapid than the transient decay in the central region of the spectrum, where a longer lived transient with absorption maxima at 420 and 450 nm is clearly detected. The time-resolved decay traces also confirm that the decay at 500 nm is relatively rapid, resulting in the complete disappearance of the transient in about 100 μs, while the decay at 420 nm is notably slower and a significant amount of transient remains 100 μs after the laser pulse, Figure 1 inset. These observations indicate that two different transient species with very distinct absorption spectra and decay kinetics are generated within the laser pulse upon 308 nm excitation of Chl in evacuated dry NaY.

From the many photochemical studies of Chl in solution, it is possible to unambiguously identify the two transients observed upon laser photolysis of Chl in evacuated NaY as the Chl triplet and the Chl radical anion, eq 1. The broad absorption between 320 and 550 nm with maxima near 360 and 500 nm is very characteristic of the Chl triplet,[60−62] while the distinctive, sharp absorption maxima at 420 and 450 nm are identical to the known absorption spectrum of the Chl radical anion.[62,63]

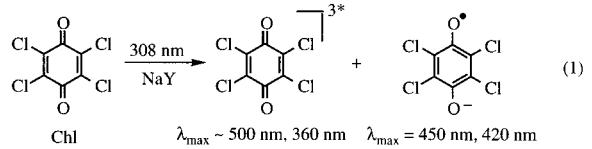

(1)

Both the Chl triplet and the Chl radical anion are the expected transients based on the characteristically rapid and efficient intersystem crossing[64] (ISC) and reduction of excited Chl in solution.[61,62] In addition, the complete decay of the Chl triplet within about 100 μs is in agreement with the reactivity of triplet states of other organic molecules such as xanthone[65] and 4-methoxy-β-propiophenone,[66] previously observed in NaY. Similarly, the long lifetime of the Chl radical anion and the persistence of considerable radical anion absorption at times longer than 1 ms are consistent with the reactivity of radical anions of pyrene[28] and 2,3,4,6-tetracyanobenzene[30] in NaY.

Further support for the identification of the Chl triplet and Chl radical anion is obtained from experiments conducted in oxygen-saturated dry NaY. Under these conditions, the bands at 360 and 500 nm are completely quenched in less than 250 ns following the laser pulse as expected for an oxygen-sensitive transient such as triplet Chl. The decay of the bands at 420 and 450 nm remains unchanged in the presence of oxygen, which is consistent with the assignment of these bands to the oxygen-insensitive Chl radical anion. A 25% decrease in the initial intensity of the bands immediately after the laser pulse is observed, indicating that less Chl radical anion is generated upon laser irradiation of Chl in oxygen-saturated NaY.

The decay kinetics of both the Chl triplet and the Chl radical anion in NaY are somewhat complex and are not first-order over the entire decay range. The decay of the Chl triplet is nicely fit using a double first-order exponential expression. This fit yields a fast decay rate constant of $(8.2 \pm 0.2) \times 10^5$ s^{-1}, comprising about 20% of the total decay, and a slower decay rate constant $(2.7 \pm 0.1) \times 10^4$ s^{-1}, which accounts for the majority, 80%, of the total Chl triplet decay in NaY. The decay kinetics of the Chl radical anion are even more complex over the observable region. Thus, while a significant fraction (30%) of the signal intensity due to the radical anion decays in the ten to hundred μs range, the remaining radical anion signal exhibits little decay over times as long as 1 ms, the longest time observable with the current laser system. Therefore, the Chl radical anion in NaY is characterized by at least two very distinct decay rate constants and more likely occurs via a distribution of rate constants about these central values. Although the slow component is too long to measure, the fast component can be fit to a single first-order expression, which yields a rate constant of $(2.1 \pm 0.1) \times 10^5$ s^{-1}.

Photoexcitation of Chloranil in NaY Containing a Secondary Electron Donor. The transient diffuse reflectance spectrum observed upon 308 nm laser photolysis of Chl (average fractional occupancy, $\langle S\rangle$ = 0.04) in evacuated NaY containing coadsorbed DMB ($\langle S\rangle$ = 0.1) is shown in Figure 2. The

characteristic absorption bands of the Chl radical anion at 420 and 450 nm, along with the shorter-lived broad absorption near 500 nm due to the Chl triplet, are clearly visible in the transient spectrum. In addition, an intense symmetrical absorption band is observed at 360 nm. As we have previously reported, this absorption is readily assigned to the 4-methoxycumyl cation that arises from rapid, within the 10 ns laser pulse, fragmentation of the DMB radical cation, the initial transient generated by Chl-photosensitized ET,[67] eq 2. The absorption spectra and decay kinetics of this transient under both vacuum and oxygen conditions are identical to the 4-methoxycumyl cation generated by direct 266 nm laser excitation of DMB within NaY.[67,68] Control experiments in which NaY-encapsulated DMB is irradiated with 308 nm laser light yield no transients, confirming that the 4-methoxycumyl cation does not arise from direct 308 nm laser excitation of DMB.

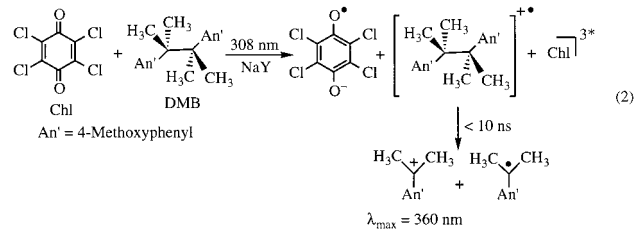

(2)

In oxygen-saturated NaY, selective excitation of Chl ($\langle S \rangle = 0.04$) containing coadsorbed DMB ($\langle S \rangle = 0.1$) likewise generates the Chl radical anion and the 4-methoxycumyl cation within the laser pulse, Figure 2, inset. The Chl triplet is no longer visible due to rapid reaction with the co-incorporated oxygen. Otherwise the transient diffuse reflectance spectrum and decay kinetics appear identical to those observed in evacuated NaY. In particular, no reduction in signal intensity due to the 4-methoxycumyl cation is observed upon the inclusion of oxygen. Similarly, the inclusion of an electron trap, nitrous oxide (vide infra), has no influence on the observed transient spectrum or decay kinetics. Unlike the results in oxygen-saturated NaY, where the Chl triplet is quenched, absorption due to the Chl radical anion, the 4-methoxycumyl cation, and the Chl triplet in nitrous oxide-saturated NaY are identical to those observed under vacuum conditions.

Figure 3 presents the results of 308 nm laser photolysis of Chl ($\langle S \rangle = 0.08$) in oxygen-saturated NaY containing increasing concentrations of DMB. The figure clearly shows that the absolute intensity of the signal at 360 nm due to the 4-methoxycumyl cation increases notably as the concentration of DMB is increased from one molecule in every 500 cavities to one molecule in every 10 cavities. This effect is consistent with a process whereby an oxidizing agent is generated upon irradiation of the zeolite-encapsulated Chl, with an increasing fraction of this oxidizing agent being trapped in the presence of higher amounts DMB to generate greater amounts of the 4-methoxycumyl cation. On the other hand, the absorption at 450 nm due to the Chl radical anion remains largely unaffected by the presence of DMB, indicating that the reduction of Chl appears to be independent of DMB content. These results provide convincing evidence that carbocation and radical anion formation show different dependencies on the amount of DMB present within the zeolite cavities.

Similar results were obtained under vacuum conditions, with the 4-methoxycumyl cation yield increasing as a function of DMB content and the Chl radical anion yield remaining largely unaffected. The effect of DMB content on the behavior of Chl triplet could also be determined under these conditions. Unlike

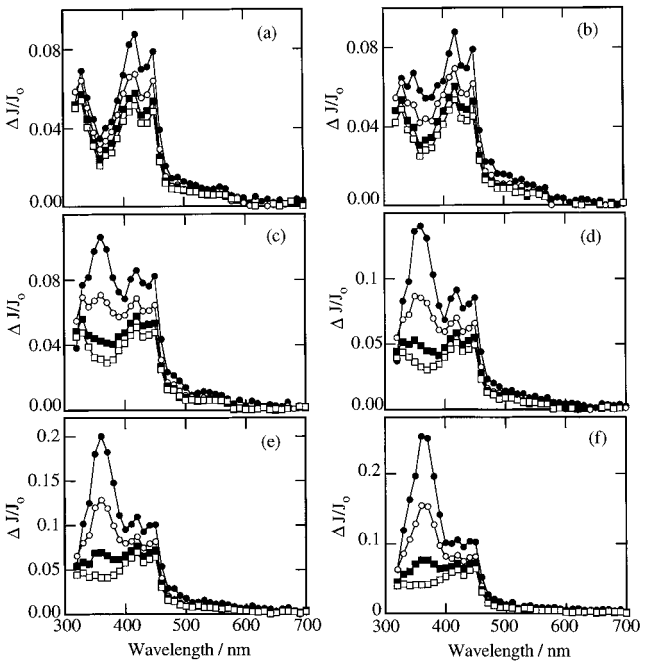

Figure 3. Transient diffuse reflectance spectra obtained 200 ns (closed circles), 1.96 μs (open circles), 6.20 μs (closed squares), and 14.0 μs (open squares) after 308 nm laser photolysis of Chl ($\langle S \rangle = 0.08$) in oxygen-saturated NaY containing various concentrations of DMB: (a) $\langle S \rangle = 0$, (b) $\langle S \rangle = 0.002$, (c) $\langle S \rangle = 0.01$, (d) $\langle S \rangle = 0.02$, (e) $\langle S \rangle = 0.04$, (f) $\langle S \rangle = 0.1$.

the results obtained for the carbocation and the radical anion, the yield of the Chl triplet decreased as the DMB content increased. The effect was significant, with the amount of triplet detected immediately following the laser pulse decreasing 60% upon going from a DMB loading level of $\langle S \rangle = 0.002$ to $\langle S \rangle = 0.10$.

While all of the spectra shown in Figure 3 were obtained with a moderately high Chl loading level of one molecule in every 12 zeolite cavities, generation of the 4-methoxycumyl cation following selective irradiation of Chl in NaY containing coadsorbed DMB is a general phenomenon observed at a variety of different concentrations of both Chl and DMB. This includes situations where the loading levels of *both* components are remarkably low. For example, at low loading levels of one Chl molecule per 50 NaY cavities and one DMB molecule per 100 cavities, distinct absorption at 360 nm due to the carbocation is still clearly observed.

Solution experiments have previously shown that Chl and various donor molecules including DMB and other bicumenes form charge-transfer complexes with broad absorption bands that extend from the UV to beyond 600 nm in the visible.[69] While such complexes could be formed in zeolites, ground-state diffuse reflectance spectra of NaY samples with various loading levels of Chl and DMB failed to show any evidence for the presence of these charge-transfer bands. In addition, laser irradiation of NaY samples containing high loading levels ($\langle S \rangle = 0.10$) of both Chl and DMB using 532 nm light, which would selectively excite any charge-transfer complex formed within the zeolite, failed to give any detectable transient species.[70] Thus, we can conclude that no detectable charge-transfer complexes between Chl and DMB are produced in our experiments and that the transients we observe are ultimately products from selectively excited Chl.

Photoexcitation of *trans*-Anethole in NaY. The transient diffuse reflectance spectrum obtained upon 308 nm laser

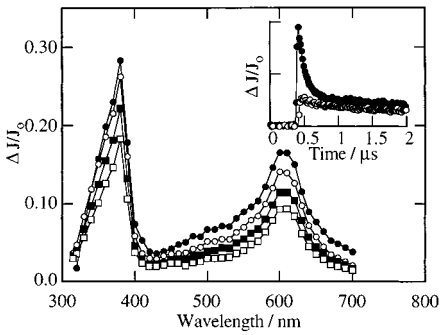

Figure 4. Transient diffuse reflectance spectrum obtained 360 ns (closed circles), 1.64 μs (open circles), 5.32 μs (closed squares), and 13.9 μs (open squares) after 308 nm laser photolysis of An ($\langle S \rangle$ = 0.1) in evacuated dry NaY. Inset shows the decay traces monitored at 700 nm following 308 nm excitation of An ($\langle S \rangle$ = 0.1) in evacuated NaY (closed circles) and nitrous oxide-saturated NaY (open circles).

excitation of An in evacuated (10^{-4} Torr) dry NaY ($\langle S \rangle = 0.1$) is characterized by intense maxima at 380 and 600 nm, Figure 4. These absorption bands are confidently assigned to the An radical cation generated by photoionization of An within the cavities of NaY, eq 3. Specifically, the transient spectrum is identical to the absorption spectrum of the An radical cation in solution,[71,72] and to that previously generated by 266 nm laser induced photoionization of An in NaY.[73] In addition, the transient species absorbing at 380 and 600 nm is unreactive toward oxygen on these time scales, consistent with the reactivity of the An radical cation.

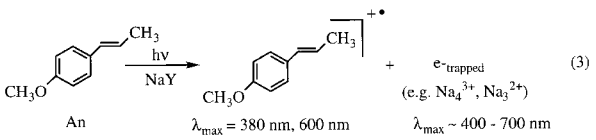

Further evidence for the photoionization reaction is obtained from the observation of sodium complexes derived from the capture of photoionized electrons by intrazeolite sodium cations.[28,73−79] These sodium ion clusters are transient species that have been identified and characterized by a combination of ESR measurements and UV−vis spectroscopic studies conducted at low temperatures and/or at fast time scales.[80] Electrons trapped by cation clusters in zeolites typically have broad, unstructured absorption in the 400 nm to 800 nm region. Within a single zeolite type the absorption maxima of sodium clusters increases with decreasing cluster size. In NaY, Na_4^{3+} has an absorption maximum near 500 nm, while smaller cation clusters, Na_3^{2+} and Na_2^{+}, have absorption maxima red-shifted to greater than 650 and 750 nm, respectively.[80] The sodium ion clusters generated upon photoionization of guest molecules are reactive species, typically decaying in the μs time regime in evacuated NaY.

The presence of broad absorption in the 400 to 700 nm region of the transient spectrum generated upon laser irradiation of An in evacuated NaY provides strong evidence for the formation of sodium-cluster trapped electrons. The decay of this absorption, Figure 4 inset, is complete within approximately 2 μs after the laser pulse, a time scale that is considerably shorter than that associated with the decay of the An radical cation. Such a short lifetime is also consistent with the presence of the trapped electron.[81,82]

The assignment of the transient absorbing between 400 and 700 nm to sodium-cluster trapped electrons is supported by

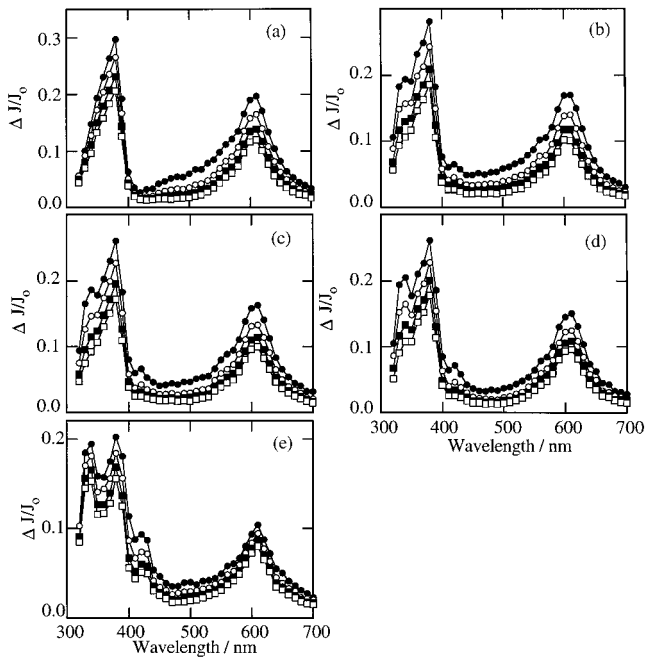

Figure 5. Transient diffuse reflectance spectra obtained 720 ns (closed circles), 3.32 μs (open circles), 8.16 μs (closed squares), and 14.8 μs (open squares) after 308 nm laser photolysis of An ($\langle S \rangle$ = 0.1) in nitrogen-saturated NaY containing various concentrations of DCB: (a) $\langle S \rangle = 0$, (b) $\langle S \rangle = 0.05$, (c) $\langle S \rangle = 0.1$, (d) $\langle S \rangle = 0.2$, (e) $\langle S \rangle = 1$.

results obtained upon the co-inclusion of electron traps. Nitrous oxide is a well-known electron scavenger and is expected to react with electrons within NaY, thereby preventing formation of trapped electron clusters.[83] Our results show that inclusion of nitrous oxide within the cavities of NaY does indeed eliminate the broad absorption in the 400 to 700 nm region. Furthermore, in nitrous oxide-saturated NaY, the decay kinetics monitored at 380 nm and especially at 600 nm are no longer contaminated by the presence of the trapped electron. Under these conditions, the decays of the two bands are virtually identical over all time regimes. The decay traces at either wavelength are a composite of more than one first-order process which are well fit by a double first-order rate expression. This yields a fast component of 3.3×10^4 s^{-1} for decay of the An radical cation in NaY that is very similar to previously reported values.[20,73] Analogous results are obtained in oxygen-saturated NaY, where quenching of the absorption due to the sodium-cluster trapped electrons by oxygen may be due to trapping of the photoejected electron by oxygen, or subsequent ET from the cluster to co-incorporated molecular oxygen.

Photoexcitation of Anethole in NaY Containing a Secondary Electron Acceptor. Transient diffuse reflectance spectra generated by 308 nm laser irradiation of An ($\langle S \rangle$ = 0.1) in evacuated NaY containing various concentrations of coadsorbed DCB are shown in Figure 5. In addition to the An radical cation with absorption bands at 380 and 600 nm, and the broad absorption due to the presence of sodium-cluster trapped electrons, a new transient species with an intense, sharp band at 340 nm and a weaker band at 430 nm is clearly formed. The transient responsible for these new absorption bands is readily identified as the DCB radical anion, based on the close resemblance of these absorption bands to the known absorption spectrum of the DCB radical anion.[72,84] Thus, 308 nm excitation of An in NaY containing DCB as a secondary electron acceptor results in the formation of the An radical cation and the DCB radical anion, eq 4.

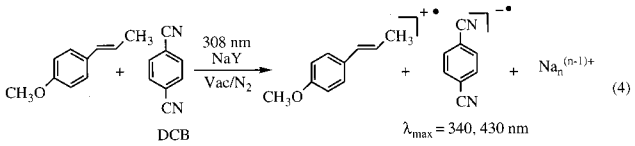

(4)

The An radical cation and the DCB radical anion are both formed promptly within the 10 ns laser pulse when An is irradiated in NaY containing DCB. The instantaneous generation of both radical ion products is observed for samples consisting of a variety of DCB and An concentrations. In each case the transient spectra are qualitatively similar, Figure 5, but distinct variations are evident in the yield of DCB radical anion and trapped electrons, Figure 6. Specifically, as the concentration of DCB is increased at a constant loading of An, the yield of DCB radical anion increases while the yield of trapped electrons decreases, Figure 6 inset. Notably, the yield of An radical cation remains essentially unaffected by the presence of DCB, except at very high concentrations of DCB ($\langle$DCB$\rangle = 1$), where a slight decrease in the An radical cation yield is observed.

As shown in Figure 7a, the inclusion of nitrous oxide, an electron trap, into the sample eliminates the absorption signals due to the DCB radical anion at 340 and 430 nm. Since the radical anion is unreactive toward nitrous oxide, the nitrous oxide must be quenching the formation of the DCB radical anion. As mentioned above, nitrous oxide traps electrons within NaY, preventing complexation of these electrons with sodium cations. In the presence of DCB a similar effect is envisioned, whereby nitrous oxide trapping of the electron intercedes the ET chemistry between An and DCB.

Elimination of the absorption bands associated with the DCB radical anion in nitrous oxide-saturated NaY is consistently observed for zeolite samples with various concentrations of DCB. However, when the loading level of DCB is very high ($\langle S\rangle = 1$), absorption due to the DCB radical anion is not completely eliminated by the co-inclusion of nitrous oxide, Figure 7b. Instead, a small shoulder remains at 340 nm, indicating incomplete quenching of radical anion formation at high DCB concentrations.

Both the An radical cation and the DCB radical anion, generated upon selective photoexcitation of An in NaY containing various concentrations of DCB, are consistently very long-lived. In all cases, the decay traces for both radical ions fit nicely to a double first-order expression yielding a fast ($k \sim 10^4$ s^{-1}) and a slow ($k \sim 10^3$ s^{-1}) decay rate constant, Table 1. While these rate constants should be regarded as an average representation of the decay kinetics of the radical ions within NaY, it is noted that the rate constants for the decay of the An radical cation monitored at 380 nm and the DCB radical anion monitored at 340 nm are quite similar for all DCB concentrations. In particular, for samples containing the highest loadings of DCB, the decay of the DCB radical anion is virtually identical to that of the An radical cation. At lower DCB loadings the decay kinetics remain quite similar, but the decay of the DCB radical anion at 340 nm appears to be slightly faster than the decay of the An radical cation at 380 nm.

Discussion

Generation of Positive Holes in Zeolites: NaY as a Single Electron Donor. Observation of the Chl radical anion upon excitation of Chl in NaY indicates that an ET reaction between excited Chl and the NaY framework is taking place and provides good evidence for the formation of positive holes within the zeolite framework. The occurrence of the ET reaction is not surprising considering results recently reported demonstrating ET from NaY to other powerful electron acceptors such as photoexcited methyl viologen ($E_{red}^* = 3.1$ V vs SCE)[14] and photoexcited cyano substituted benzenes ($E_{red}^* \sim 3.1-2.5$ V vs SCE).[30] In addition, since the formation of the Chl radical anion is instantaneous on the time scales examined, a lower limit for the rate constant for ET from NaY to photoexcited Chl can be set at ca. 1×10^8 s^{-1}. Therefore, these results demonstrate ultrafast ET from NaY to photoexcited Chl and provide additional experimental evidence that the zeolite can participate as an electron donor in PET reactions with encapsulated guest molecules.

In addition to the Chl radical anion, the Chl triplet is also observed immediately following laser excitation of Chl in evacuated NaY. The triplet decays on the μs time scale, but this decay is not accompanied by formation of the Chl radical anion. The absence of radical anion formation on this time scale indicates that the long-lived observable triplets do not react via slow reduction by the NaY framework. Thus, some of the excited-state Chl molecules abstract an electron from the zeolite framework in less than 10 ns, while other Chl molecules deactivate from the triplet state via alternative reaction pathways.

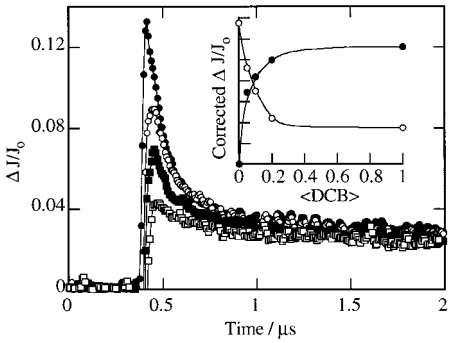

Figure 6. Decay traces monitored at 700 nm following 308 nm laser photolysis of An ($\langle S\rangle = 0.1$) in nitrogen-saturated NaY containing coadsorbed DCB: $\langle S\rangle = 0$ (closed circles), $\langle S\rangle = 0.05$ (open circles), $\langle S\rangle = 0.1$ (closed squares), $\langle S\rangle = 0.2$ (open squares). Inset shows the variation in the yield of DCB radical anion (closed circles) and sodium-cluster trapped electrons (open circles) as a function of DCB occupancy.

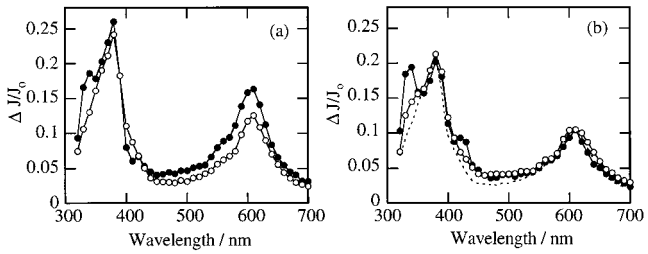

Figure 7. Transient diffuse reflectance spectra obtained 720 ns after 308 nm laser photolysis of An ($\langle S\rangle = 0.10$) in nitrogen-saturated (closed circles), and nitrous oxide-saturated (open circles) NaY containing coadsorbed DCB: (a) $\langle S\rangle = 0.1$, and (b) $\langle S\rangle = 1$. The spectrum of the anethole radical cation (dashed line) is included in (b) to highlight the residual DCB radical anion signal under nitrous oxide conditions.

TABLE 1: Rate Constants for the Decay of the An Radical Cation at 380 nm and DCB Radical Anion at 340 nm in Evacuated NaY ($\langle$An$\rangle = 0.1$)

	$k_{fast}/10^4$ s^{-1}		$k_{slow}/10^3$ s^{-1}	
$\langle$DCB$\rangle$	380 nm	340 nm	380 nm	340 nm
0.05	3.94 (64%)	4.72 (67%)	1.54 (36%)	3.31 (33%)
0.1	3.38 (50%)	3.71 (67%)	3.39 (50%)	3.10 (33%)
0.2	3.36 (49%)	3.21 (67%)	2.55 (51%)	2.51 (33%)
1	2.88 (37%)	2.75 (39%)	2.08 (62%)	2.13 (61%)

SCHEME 1

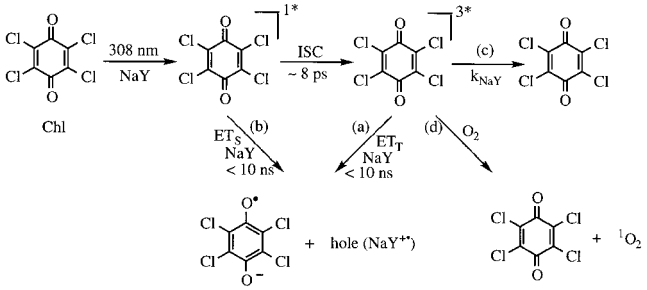

Electron transfer from the framework to photoexcited Chl is therefore either very rapid (<10 ns) or does not occur at all within the lifetime of the triplet state (~100 μs).

One explanation that accounts for these observations is that the zeolite microenvironment possesses a distribution of oxidation sites of varied potentials. Chl molecules in close proximity to strong donor sites are rapidly reduced upon photoexcitation, each generating a Chl radical anion as well as a positive hole in the zeolite framework. Other Chl molecules not interacting with sites of sufficient oxidation potential do not participate in ET reactions with the NaY framework. This is analogous to descriptions of photoexcited donors such as pyrene and anthracene within NaY,[74,75,77] whereby those photoexcited species in close proximity to a strong electron accepting site undergo ionization, while those species distant from such a site undergo different reactions such as ISC to the triplet state. In addition, it is also possible that some of the Chl radical anions formed come from singlet Chl instead of triplet Chl, as the Chl singlet ($E_{red}^* = 2.77$ V vs SCE) is an even more powerful oxidant than the Chl triplet ($E_{red}^* = 2.15$ V vs SCE).[64] Based on these considerations, it is not unreasonable to suspect that ET from NaY to singlet Chl accounts for a fraction of Chl radical anion formation.

A summary of the processes discussed above representing the behavior of photoexcited Chl in NaY is shown in Scheme 1. The initial transient generated upon 308 nm laser excitation of Chl within NaY is the Chl singlet, which is not detected due to rapid ISC to the Chl triplet.[64] In less than 10 ns the Chl radical anion is generated by ET from the zeolite framework to the Chl triplet, Scheme 1 path (a), and perhaps also to the Chl singlet, path (b). The Chl triplets observed following the laser pulse do not decay via ET, but instead decay in the μs time regime under vacuum, most likely through deactivation to the ground state, path (c). In oxygen-saturated NaY, the Chl triplet is partially quenched, path (d), resulting in a concomitant reduction in the yield of Chl radical anion, path (a). Because paths (a) and (b) leading to the radical anion are so rapid, or involve Chl molecules inaccessible to oxygen, only partial oxygen quenching of Chl radical anion formation is observed.

The generation of the Chl radical anion upon photoexcitation of Chl within the cavities of NaY indicates that an electron is transferred from the zeolite framework to the Chl molecule. A possible source of electron density for donation to a photoexcited acceptor is the lone pair of electrons on the bridging lattice oxygen atoms, particularly those in [Si−O−Al]$^-$ sites. Studies of electron donation from NaY to included organic acceptors are consistent with this notion. For instance, photoreduction of pyrene within the cavities of alkali metal cation X and Y zeolites has been proposed to involve donation from oxygen atoms within [Si−O−Al]$^-$ bridges.[14,28] This proposal is supported by the observation that enhancing the electron density at this site by increasing the alkali cation size or decreasing the Si/Al ratio increases the relative yield of radical anion formation. In fact, the yield of pyrene radical anion was found to correlate nicely with the charge on the zeolite framework oxygen atom as determined by Sanderson electronegativity.[28] Furthermore, recent EPR investigations of the thermal formation of *o*-Chl radical anions in cesium acetate impregnated CsX and CsY zeolites suggest that the positive hole generated upon electron donation is localized on the oxygen atoms adjacent to the aluminum centers.[85] Based on the results of these studies, it is most likely that the dominant electron donating sites responsible for reduction of photoexcited Chl in NaY are the lattice oxygen atoms within [Si−O−Al]$^-$ bridges, eq 5.

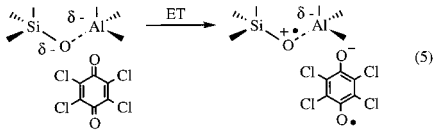

In light of this discussion, it is interesting to consider the time-resolved decays of the Chl radical anion. Under oxygen, in the absence of any triplet absorption, the radical anion decay exhibits at least two distinct components. Along with a very long-lived component, a considerably faster decay is also visible. These distinctly different rate constants for radical anion decay may be related to the heterogeneity of the zeolite interior and redox sites of varied strength. Radical anions generated by weaker donor sites might undergo BET on observable time scales, while those associated with more oxidative sites might resist BET long enough for either the radical anion or the hole to escape. It is also possible that the existence of both singlet and triplet radical ion pairs could play a role in the significant variations in the radical anion lifetime.

Regardless of the observed variation in decay rate constants, the substantial lifetime of the Chl radical anion generated by PET from NaY is clear, with a significant fraction of the transients showing no decay over more than 800 μs. Experiments involving framework donation to zeolite-incorporated methyl viologen[14] or 1,2,4,5-tetracyanobenzene[30] have also observed significant lifetimes for the ET products. The explanation for this behavior is likely related to rapid and persistent separation of the initially formed radical ion pairs to generate long-lived charge separated species that are quite resistant to BET. Favorable electrostatic stabilization provided by the highly polar environment within zeolite cavities is one factor that contributes to the long lifetime of the radical ion pairs. More importantly, spatial separation whereby the hole migrates to an adjacent cavity and beyond is also likely to play an important role in defining the lifetime of the radical ion pair.

Mechanism(s) for Intrazeolite Electron Transfer Following Selective Excitation of an Electron Acceptor in NaY. Every molecule of Chl that abstracts an electron from NaY produces a corresponding positive hole in the framework. One means of probing these zeolite holes is to generate them in the presence of a secondary electron donor with which they might react. Selective photoexcitation of Chl in NaY containing coadsorbed DMB yields the Chl triplet, the Chl radical anion, and the 4-methoxycumyl cation immediately following the 308 nm laser pulse. Since the 4-methoxycumyl cation originates from fragmentation of the DMB radical cation within the laser pulse, the observation of the 4-methoxycumyl cation indicates that the DMB radical cation is generated upon laser excitation of Chl in NaY containing coadsorbed DMB. Direct 308 nm photoexcitation of DMB is not responsible for the formation of the DMB radical cation, as DMB does not absorb at 308 nm. In addition,

SCHEME 2

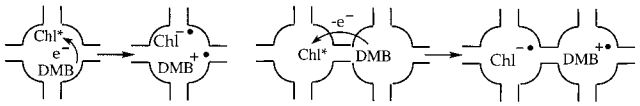

SCHEME 3

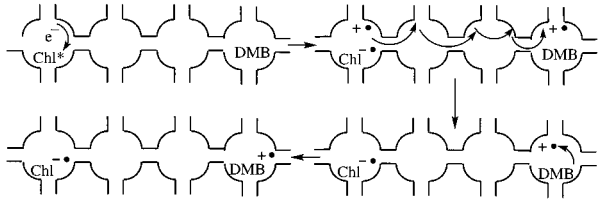

no evidence could be found for the presence of a Chl/DMB charge-transfer complex within NaY. Thus, the DMB radical cation must arise from reactions initiated by photoexcited Chl within NaY.

Two distinct mechanistic schemes can be applied for the formation of the DMB radical cation upon photoexcitation of Chl in NaY containing coadsorbed DMB. The first involves direct ET from ground-state DMB to photoexcited Chl. Depending on the rate constant for ET in NaY, this process could involve either singlet or triplet Chl, generating the corresponding singlet and triplet radical ion pairs. The resultant radical ion pairs could decay back to the ground state via BET, or if BET is sufficiently slow, the DMB radical cation may undergo fragmentation to the 4-methoxycumyl cation as observed experimentally. This ET mechanism, as represented in Scheme 2, would most likely involve a direct interaction between photoexcited Chl and a DMB molecule in close proximity, either within the same cage or in a neighboring cage.

Alternatively, the formation of the Chl radical anion upon photoexcitation of Chl in NaY containing no DMB suggests that another mechanism may exist for the formation of the DMB radical cation. In this case, ET from NaY to photoexcited Chl to generate the radical anion and a hole in the framework continues to take place in the presence of DMB. Migration of this hole to a cavity containing DMB followed by ET from the DMB to the zeolite hole then generates the DMB radical cation, and correspondingly, the 4-methoxycumyl cation, within the laser pulse, Scheme 3.

The experimental results suggest that both mechanisms, direct ET quenching of excited state Chl by DMB, Scheme 2, and hole migration to isolated DMB, Scheme 3, are responsible for the observed redox chemistry. One piece of evidence for hole migration comes from the reaction sphere calculations described below. Other evidence includes the fact that detectable amounts of the 4-methoxycumyl cation are formed even at very low loading levels of both Chl and DMB within NaY. Under these conditions few, if any, Chl and DMB molecules will be sufficiently close together for direct ET to occur.

As well, the mobility of these large guests through the zeolite pores and cavities should be slow, and it is unlikely that migration of excited Chl to a cavity containing DMB, or migration of a DMB molecule to a cavity containing excited Chl, is sufficiently rapid to account for the observed ET. On the other hand, holes created by ET from the framework to excited Chl would have a much greater ability to migrate away from the cavity containing the initially excited Chl. As a result, the probability that a DMB located in a remote cavity will encounter a strong oxidizing hole will be considerably increased.

The observation that the yield of carbocation increases as a function of increasing DMB content while the Chl radical anion yield remains essentially unchanged is also consistent with a mechanism involving photogenerated holes. According to this mechanism, hole and Chl radical anion formation do not require the presence of DMB and hence will be independent of DMB content. However, the fraction of holes trapped by DMB will increase with increasing DMB content, thus leading to an increased yield of carbocation.

SCHEME 4

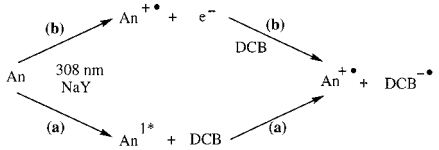

The observation that the yield of triplet Chl decreases as a function of increasing DMB content suggests that some direct ET is also taking place. This can occur from either the triplet manifold or the singlet manifold. In the case of quenching of triplet Chl, direct ET would result in triplet Chl being converted to the Chl radical anion, thus leading to an increased yield of the radical anion as a function of increasing DMB content. Alternatively, singlet radical ion pairs would be generated if the direct ET involved singlet Chl. In this case, BET to generate ground state species would occur competitively with carbocation formation by cleavage of the initially formed DMB radical cation. As a result, singlets that would otherwise have intersystem crossed to triplet Chl are removed, causing the triplet yield to decrease with no corresponding increase in Chl radical anion formation.

Mechanism(s) for Intrazeolite Electron Transfer Following Selective Excitation of an Electron Donor in NaY. The experimental results described earlier clearly demonstrate that photoexcitation of An in NaY containing coadsorbed DCB leads to the generation of the An radical cation and the DCB radical anion within the 10 ns laser pulse. Again, two mechanistically distinct pathways can be envisioned for DCB radical anion formation following photoexcitation of An in the presence of DCB. The first involves a PET reaction whereby an electron is transferred to a DCB acceptor in close contact with an excited-state An donor, Scheme 4 path (a). The second involves photoionization of the An donor, as observed in the absence of DCB, followed by subsequent trapping of the electron by a DCB molecule elsewhere within the zeolite matrix, Scheme 4 path (b).

It is expected that direct PET will play a role in radical ion generation, particularly at high loadings where the probability of double cage occupancy and occupancy of adjacent cages is quite high (vide infra). However, the experimental results do not suggest that direct PET is the major pathway for generation of the radical ions detected in the nanosecond time-resolved experiments. For instance, the notion that photoionization, rather than direct PET, continues to be the dominant mechanism for An radical cation generation in the presence of DCB, is supported by the fact that the yield of An radical cation remains approximately constant for a single An concentration, regardless of DCB concentration. This indicates that enhanced generation of An radical cations by PET with DCB, Scheme 4 path (a), does not occur upon laser excitation of An in NaY with coadsorbed DCB, or that those additional radical ions generated by direct ET quenching are not observed due to rapid BET. A slight decrease in the yield of An radical cation is evident at the extremely high loading of one DCB molecule per cavity. Under these circumstances, direct ET quenching is likely competitive with photoionization. Some of the singlet radical ion pairs generated in this way will separate to give An radical

SCHEME 5

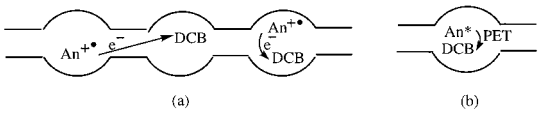

cation and DCB radical anion. However, most will undergo BET to regenerate the ground-state starting materials, thus leading to a decreased efficiency in the conversion of An to the An radical cation.

More convincing evidence that photoionization followed by electron migration and trapping, Scheme 4 path (b), is the significant mechanism for radical anion generation is obtained from experiments employing nitrous oxide. In the presence of nitrous oxide no DCB radical anions are detected after laser photolysis of An in NaY containing less than $\langle S \rangle = 1.0$ DCB, Figure 7a. This observation is consistent with a mechanism whereby nitrous oxide scavenges the photoionized electron before it can be captured by DCB, therefore inhibiting radical anion formation. An obvious interpretation of this result is that the electron must travel a finite distance between photoexcited An and DCB in order to be intercepted by nitrous oxide, Scheme 5a. The fact that DCB radical anion formation is not completely quenched by nitrous oxide at very high loading levels, Figure 7b, where some detectable ion pairs are likely formed by direct PET indicates that this process is not affected by nitrous oxide, Scheme 5b. This observation reinforces the conclusion that nitrous oxide quenching involves capture of the photoionized electron within the zeolite environment.

Since experimental investigations of hole migration employed an electron donor, DMB, whose radical cation undergoes rapid fragmentation, BET reactions that are slower than C−C bond cleavage cannot be monitored using nanosecond diffuse reflectance spectroscopy. However, for the An/DCB redox pair, the primary redox products are spectroscopically observable on the nanosecond time scale, and the corresponding decay rate constants can be obtained, Table 1. The similarity between the rate constants for decay of the DCB radical anion and the An radical cation suggests that the decay mechanism of the radical ions most likely involves mutual annihilation via BET to regenerate ground-state An and DCB. Notably, the greatest similarity in the rate constants for decay of the two radical ions is found at the highest concentration of DCB where some detectable radical ions must be formed by direct PET. At lower concentrations of DCB the decay of the radical anion is slightly faster than the decay of the radical cation, indicating that direct BET may not be the only mechanism for radical ion decay when the ion pair is more dispersed within the zeolite network.

It is also significant to note that the radical ions are very long-lived, decaying over hundreds of microseconds and longer, with decay rate constants on the order of 10^4 and 10^3 s^{-1} for both the An radical cation and DCB radical anion. The long lifetimes of these radical ions indicate that the zeolite environment provides a significant degree of stabilization to the charge-separated species. Although similarly long-lived charge-separated states have previously been reported, in these cases, either the electron acceptor[26,27] or both the electron donor and the electron acceptor[43,45] were positively charged species within zeolites. It is expected that strong Coulombic interactions will exert distinct influences on the starting reagents, as well as the radical cation pair generated by PET in these systems, as compared to the radical cation−radical anion pair generated by PET between two neutral species. In fact, Hashimoto et al. recently reported rate constants of ca. 10^7 to 10^9 s^{-1} for BET between contact radical ion pairs generated by PET in charge-transfer complexes consisting of neutral species.[57] Although the BET was slowed by approximately 1 order of magnitude compared to solution, the results indicate that BET between contact ion pairs within zeolites can be rapid. In light of these observations, the long lifetime of the An radical cation−DCB radical anion pair further supports the notion that these species achieve enhanced stabilization due to their spatial separation within the zeolite.

Estimating the Distance of Electron and Hole Migration in Zeolite NaY. The experimental results presented suggest that both electron and hole migration can occur between electron donors and acceptors spatially separated within the zeolite matrix. To provide further evidence for this possibility, it is necessary to establish that the observed redox products cannot be accounted for strictly by contact interactions and to estimate the intrazeolite distances for electron and hole migration. Thus, the experimental data concerning the yields of redox products as a function of the concentration of redox reagents are examined herein using two independent models.

Perrin Model. The Perrin model[86−88] is often used to describe quenching of an excited-state species in situations where motion is not possible within the excited-state lifetime. In this approach, the excited state is imagined to be surrounded by an "active-sphere" of volume, *V*, and radius, *r*. If the quencher is present within this sphere, then quenching will take place instantaneously with unit efficiency. However, if the quencher is outside the active sphere, quenching will not take place and the excited species decays as it would in the absence of quencher. In its most general form, the Perrin model predicts a logarithmic decline in emitter intensity with increasing quencher concentration, eq 6,

$$\ln(\Phi_o/\Phi) = VN[Q] \qquad (6)$$

where Φ_o and Φ are the quantum yields of emission in the absence and the presence of quencher respectively, *V* is the volume of the active quenching sphere, equal to $4\pi r^3/3$, and *N* is Avogadro's number. The Perrin model has previously been applied by Dutta et al. to determine a quenching radius of 13 Å for ET between photoexcited $Ru(bpy)_3^{2+}$ and methyl viologen in NaY.[89] As this value is very close to the sum of the molecular radii of the molecules involved, the quenching was proposed to proceed via molecular contact mediated through the zeolite pores. Similarly, Thomas et al. used the Perrin model to predict distances of 13.6 and 11.1 Å for ET quenching of excited-state pyrene by metal ions, Cu^{2+} and Tl^+, respectively, in zeolite X.[58,59] In addition, Thomas and co-workers have extended the Perrin model to include reactions in zeolites that do not involve excited-state species, using it to estimate a distance of 30 Å for migration of the hydrated electron within NaY zeolites to a methyl viologen trap.[81] In applying the Perrin model to the current system, the electron or hole, initially generated by PET involving the NaY framework, is considered to be surrounded by a reaction sphere of radius, *r*, the magnitude of which defines the distance of charge migration. If a secondary redox partner is within the quenching sphere, trapping will take place and the oxidized or reduced transient will be detected. Conversely, if the secondary redox partner is outside the sphere, the electron or hole will not be trapped and the corresponding oxidized or reduced transient will not be experimentally observed.

Experimental results concerning hole migration between photoexcited Chl and DMB indicate that the yield of the redox product, the 4-methoxycumyl cation, increases as the concentration of DMB is increased at a constant concentration of Chl, Figure 3. In this case, the quantity being considered is formed

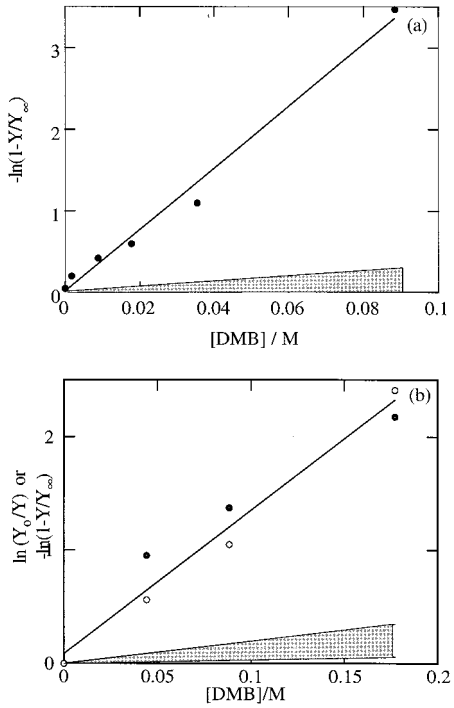

Figure 8. (a) Perrin plot of $-\ln(1 - Y/Y_\infty)$ against DMB concentration, where Y represents the yield of the 4-methoxycumyl cation in NaY. The shaded region indicates the behavior expected for DMB and Chl molecules in direct contact. (b) Perrin plots of $-\ln(1 - Y/Y_\infty)$ where Y represents the yield of the DCB radical anion (closed circles) and $\ln(Y_0/Y)$ where Y represents the yield of the trapped electron (open circles) in NaY. The shaded region indicates the behavior expected for DCB and An molecules in direct contact.

by the reaction of interest, rather than being quenched. Therefore, the Perrin model predicts an exponential increase in the yield of the 4-methoxycumyl cation as a function of quencher concentration, eq 7,

$$Y/Y_\infty = 1 - \exp(-VN[Q]) \tag{7}$$

where Y and Y_∞ represent the observed yield of product formed in the reaction and the maximum possible yield of product in the reaction, respectively.[90] Rearranging eq 7 gives an equation analogous to the general Perrin formula, eq 8.

$$-\ln(1 - Y/Y_\infty) = VN[Q] \tag{8}$$

Plotting the experimental data according to eq 8, where Y represents the yield of the 4-methoxycumyl cation obtained from the transient diffuse reflectance experiments[91] and [Q] represents the concentration of DMB in NaY in moles per liter, yields a nicely linear correlation in accord with the Perrin model, Figure 8a. Similar plots are observed for other data sets in which the Chl loadings were varied from $\langle S \rangle = 0.02$ to $\langle S \rangle = 0.08$. In each case the slopes of the plots match fairly well, and the average radius for the reaction sphere is determined to be (27 $\pm$ 2) Å. This is significantly larger than the sum of the molecular radii of the molecules.[92] In fact, as shown by the shaded region in Figure 8a, the slopes of the Perrin plots would have been dramatically more shallow if the reaction was restricted to contact interactions between these two molecules (i.e., Perrin reaction radius equal to the sum of the molecular radii).

A similar analysis was carried out for the An/DCB system. In this case it is possible to examine both the yield of the product formed in the redox reaction, the DCB radical anion, according to eq 8, as well as the yield of the electron quenched by the reaction, according to eq 6, where quantum yield is replaced by transient yield, Y. The yields of both the DCB radical anion and zeolite trapped electron exhibit variations predicted by the Perrin model, and very similar reaction sphere radii are obtained from both sets of data, Figure 8b. The average reaction radius obtained from the radical anion and electron yields in two independent trials is (18 $\pm$ 2) Å. Again this reaction radius is considerably larger than the sum of the molecular radii,[92] and the slope of the Perrin plot predicted for ET due to contact interactions (shaded region Figure 8b) is notably more shallow than the experimental slopes.

Distribution Model. In solution and in many types of heterogeneous media, a continuum of intermolecular distances between reagents is possible. In contrast, the regular structure of zeolites restricts possible intermolecular distances to discrete values defined by the number of unfilled cages between molecules. In addition, relatively large organic molecules cannot move within the cage and channel structure of the zeolite on the time scales of chemical reactions such as PET. Due to the specific, well-defined structural arrangement of adsorbates, it is possible to formulate a simple model of the molecular distribution and hence intermolecular distances between adsorbates in zeolites. Such an approach to mapping the distribution of adsorbates within zeolites has been adopted by Dutta and co-workers to understand intermolecular interactions between $Ru(bpy)_3^{2+}$ encapsulated within NaY.[93] We have likewise applied this distribution model to describe the distribution of electron donors and acceptors in NaY and help interpret the intrazeolite redox chemistry.

To describe the intrazeolite distribution of adsorbates in NaY, first consider an arbitrary supercage, **a**, which, due to the tetrahedral arrangement of cavities within Y zeolites, will be surrounded by four neighboring supercages, denoted **b**. As the diameter of each supercage is approximately 13 Å, the distance from the center of supercage **a** to the center of any **b** supercage is about 13 Å. Therefore, the centers of the four **b** supercages are equidistant from the center of supercage **a** and form a "shell", shell **b**, with a radius of 13 Å. Likewise, each of the four supercages in shell **b** has three additional neighbors that are also equidistant from supercage **a**. These 12 supercages generate a third shell, shell **c**, which is approximately 21 Å from the center of shell **a**. A series of successive shells and the distance of these shells from the central supercage **a** can similarly be constructed. From the radius of each shell and the size of adsorbed molecules it is possible to estimate the intermolecular distances between a reagent in supercage **a** and a reagent in any of the supercages comprising the surrounding shells, Table 1S.

To map the distribution of molecules within the NaY matrix it is necessary to determine the occupancy probability of cavities within each shell as a function of adsorbate concentration. Consider, for example, NaY samples containing a constant concentration of Chl and varied concentrations of DMB. Starting with a single supercage **a**, that is occupied by a Chl molecule, the probability that a DMB molecule will be within the cavities of adjacent shells can be determined using the concentration of DMB, assuming that the distribution of DMB is not influenced by the presence of Chl. For a DMB concentration of one molecule in every 10 cavities ($\langle S \rangle = 0.1$), the probability that any single cavity is occupied by DMB is 0.1 and the probability that a single cavity does not contain DMB is 0.9. The probability that DMB is not present within any of the four cavities of shell **b** is $(0.9)^4$ or 0.656, and therefore the probability that one or more of the cavities in shell **b** is occupied by a DMB molecule

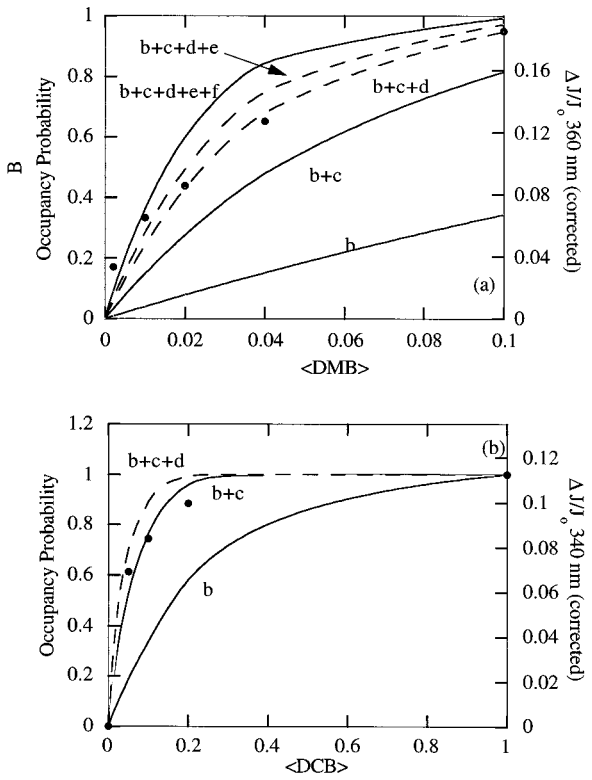

Figure 9. (a) Experimental variation in the yield of the 4-methoxycumyl cation (closed circles) determined from the corrected Δ.O. D. at 360 nm as a function of the fractional occupancy of DMB in NaY compared to the variation predicted by the distribution model (lines). The experimental data have been normalized to the sum of shells **b** + **c** + **d**. (b) Experimental variation in the yield of the DCB radical anion (closed circles) determined from the corrected Δ.O. D. at 340 nm as a function of the fractional occupancy of DCB in NaY compared to the predicted variation (lines). The experimental data have been normalized to the sum of shells **b** + **c**.

is 0.344. For shell **c**, the total number of cavities surrounding cavity **a** are the 16 cavities comprising both shells **b** and **c**. The probability that none of the 16 cavities contain DMB is (0.9),[16] or 0.185. Therefore, the probability that at least one is occupied by DMB is 0.815. The probability that this occupancy is in shell **c** can be obtained by subtracting the probability of shell **b** occupancy, 0.344, from the total probability of occupancy, 0.815, to give 0.471 as the occupancy probability of shell **c** at a DMB occupancy level of 0.1. Similarly, the probability that each successive shell is occupied by DMB can be determined until the majority of molecules are accounted for. Table 2S presents the calculated occupancy probabilities for successive shells at various concentrations of DMB within NaY, and Table 3S presents similar results for various concentrations of DCB within NaY.

The distribution of reagents obtained from this model can be used to rationalize interactions between adsorbates and, for the current results, to obtain estimates for the distance of electron or hole migration within the cavities of NaY. Consider first hole migration between photoexcited Chl and DMB within the NaY matrix. Comparing the yield of hole migration (i.e., the yield of 4-methoxycumyl cation) as a function of DMB concentration with the DMB occupancy probability as a function of DMB concentration relates the efficiency of hole migration to separation distance. Such a comparison is shown in Figure 9a, which plots the observed yield of carbocation and the summed occupancy probability of several shells from a central supercage, **a**. These plots demonstrate that hole migration is not limited to adjacent cavities, shell **b**. Likewise, the hole can clearly travel farther than shell **c** since the data normalized to the sum of shells **b** and **c** are very poor (sum of the square of residuals is 0.048). The best correlation between the observed data and the summed occupancy of shells is obtained for shells **b** through **d** (sum of the square of residuals is 0.022) and for shells **b** through **e** (sum of the square of residuals is 0.024). Including the occupancy of shell **f** worsens the correlation (sum of the square of residuals is 0.058). The direct through-space distance between the central supercage **a** and shells **d** and **e** corresponds to 24 and 30 Å, respectively. However, when the molecular sizes of Chl and DMB are considered, by using half the largest molecular dimension in each case, the vacant through-space distance for hole migration is estimated to be between 14 and 19 Å.

Analogous comparisons can be made for electron migration between photoexcited An and DCB. Thus, comparing the yield of electron migration (i.e., the yield of the DCB radical anion) as a function of DCB concentration with the DCB occupancy probability as a function of concentration gives an indication of the efficiency of electron migration as a function of intermolecular separation. The comparison confirms that the interactions leading to the observed ET chemistry are not solely contact interactions and do not correlate to electron motion only to neighboring cages, shell **b**, Figure 9b. For this system, the experimental data fit best to the summed occupancy probability of shells **b** and **c**, suggesting that the electron can traverse at least one unoccupied NaY cavity. The direct through-space separation from the center of supercage **a** to the center of a cavity in shell **c** corresponds to 21 Å. Subtracting half the longest interatomic distances of An and DCB from this value yields 12 Å as an estimate for the vacant through-space distance for electron migration between An and DCB in NaY.

The above discussion indicates that a model based on the distribution of reagents within zeolites can provide useful information concerning the interactions of adsorbates. It must be acknowledged that the data do not fit exactly to the model, indicating that the model and/or assumptions used to obtain the distribution for the mixed adsorbate systems may be improved. Overall, however, the data determined for the two unique systems employed to study electron and hole migration are fit reasonably well by the distribution model. Furthermore, the similarity of the predictions derived from this model to those obtained from the Perrin treatment lends support to the validity of both models. Thus, both models predict that the total distances traveled by the hole and the electron are in the range of 24 Å to 30 Å and 18 Å to 21 Å, respectively. Average distances obtained by considering both models are 28 Å for hole migration, Scheme 6 (a), and 20 Å for electron migration, Scheme 6 (b). Incorporation of the molecular dimensions of the specific reagents within each model allows the extraction of explicit periphery−periphery distances and therefore the unoccupied space within the zeolite cavities through which the hole and electron travel. The resultant predictions derived from the distribution model are 14 Å to 19 Å for hole migration and 12 Å for electron migration. If it is assumed that at least half of the quencher molecule must be contained within the Perrin reaction sphere in order for reaction to take place, estimates of 18 Å for hole migration and 9 Å for electron migration are obtained. Thus, the average vacant space distances for hole and electron migration derived from consideration of both models are 18 Å and 11 Å, respectively.

It is important to emphasize that regardless of the exact estimates of the distance traveled by electrons and holes, the experimental results demonstrate that the observed redox

SCHEME 6

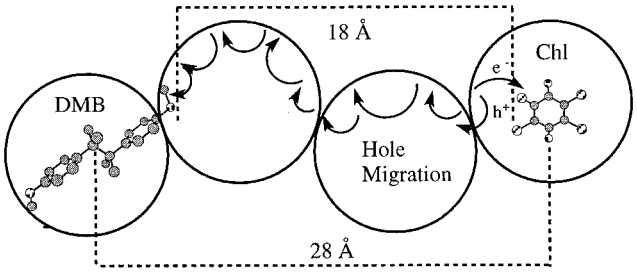

(a)

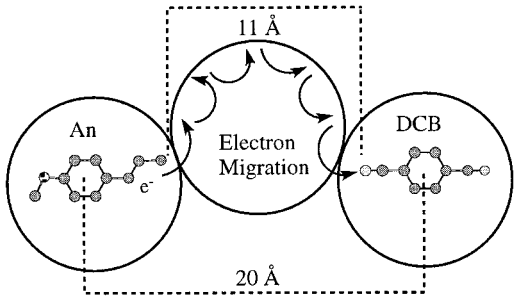

(b)

reactions cannot be accounted for through contact interactions alone. This does not imply that species in molecular contact do not exist, nor that such contact interactions do not lead to ET reactions and generate the observed products. However, in addition to these interactions, chemistry over longer distances must be taking place, at a variety of distances up to the maximum values predicted by the models. As such, the zeolite is thought to mediate these more distant processes, actively participating in the migration of charge between the donor and acceptor. In this regard it must also be recognized that the distances predicted by both models refer to direct through-space distances. This likely does not accurately represent the mechanism by which the charge migrates through the zeolite. More likely the hole and the electron migrate, or hop, along the zeolite framework from the site of origin to the secondary redox partner, as depicted in Scheme 6. For instance, the hole may move along electron-rich framework sites such as oxygen atoms within $[Si-O-Al]^-$ bridges, while the electron may move along electron deficient sites such as cations, cation clusters, or aluminum centers. For charge migration proceeding along the framework, the total distance traveled is likely significantly longer than the direct through-space distance.

Conclusions

The current investigation provides direct evidence that NaY zeolites can participate as both electron acceptors and electron donors in PET reactions with included organic reagents. Zeolite encapsulation also facilitates bimolecular ET reactions between coadsorbed guest molecules, leading to long-lived charge separated states confined within the zeolite matrix. In addition, the experimental results indicate that intrazeolite ET chemistry can take place between spatially separated reagents. The ET reactions observed in the absence of intermolecular contact are proposed to be mediated by the intervening zeolite framework and can more accurately be represented as electron or hole migration rather than direct ET quenching of excited states. These results have been interpreted using two independent models in order to estimate distances of 18 and 11 Å for migration of a hole and an electron, respectively, through intrazeolite space. The results presented herein are based on experimental studies that have been applied successfully to two donor−acceptor systems. We are currently conducting additional experiments employing other molecular systems to establish the generality of the phenomenon as well as the validity of the interpretation and the reliability of the experimental models. This too will hopefully shed some light on the mechanisms of these charge migration reactions and the factors that influence the migration distance.

Experimental Section

Materials. Chloranil, *trans*-anethole and 1,4-dicyanobenzene were commercially available from Aldrich. 1,4-Dicyanobenzene was recrystallized from 95% ethanol prior to use. 4,4′-Dimethoxybicumene was prepared according to the literature procedure,[94] purified by sublimation, and fully characterized using ^1H and ^{13}C NMR spectroscopy. NaY, LZY52 molecular sieves Si/Al = 2.4, was obtained from Aldrich and used after activation at 450 °C for at least 12 h to remove coadsorbed water. Spectroscopic grade solvents (<0.02% water) used in zeolite sample preparation were commercially available (OmniSolv, BDH) and were used without additional purification.

Zeolite Samples. A general procedure for the preparation of single adsorbate zeolite samples is as follows. Zeolites (typically 300 to 400 mg) were activated for at least 12 h at 450 °C to remove the coadsorbed water. The dehydrated zeolite was removed from the oven and immediately placed in approximately 20 mL of anhydrous hexane in a sample tube and sealed with a septum. A small quantity (typically < 250 μL) of a relatively concentrated (typically 10^{-1} to 10^{-2} M) hexane or dichloromethane solution containing the compound of interest was then added to the zeolite−hexane slurry, the mixture was stirred for 1 to 2 h, and then the carrier solvent was separated from the zeolite solid by centrifugation. An additional 20 mL aliquot of hexane was added to the solid material, and the mixture was again stirred for approximately 30 min to remove surface adsorbates, centrifuged, and the zeolite sample was separated from the supernatant liquid. To remove the remaining hexane, the zeolite−substrate complex was placed in a desiccator which was evacuated with a vacuum pump (10^{-3} Torr) for 8 to 12 h. The sealed desiccator containing the zeolite powder was placed in a glovebag under an atmosphere of dry nitrogen in order to transfer the dried zeolite composite to a 3 × 7 mm^2 quartz laser cell. This cell was attached to a vacuum line equipped with a diffusion pump (10^{-4} Torr) for an additional 12 h to remove any oxygen and any residual hexane that may have been present.

Zeolite samples containing two adsorbates were prepared by incorporating the two molecules separately. In most cases a series of samples were prepared containing a constant concentration of the adsorbate to be photoexcited and a variable concentration of the other adsorbate. The fixed concentration adsorbate was first included within a large batch of activated zeolite. This procedure was analogous to the description given above, aside from the fact that it was conducted on a larger scale (ca. 5−6 fold increase). Typically 1 to 2 g of activated zeolite, 120 mL aliquots of anhydrous hexane, and stirring periods of 3 to 4 h were employed. After removing the hexane by vacuum pumping (10^{-3} Torr) in a desiccator for approximately 12 h, the initial zeolite−adsorbate composite was divided into preweighed sample tubes and sealed with septa under an atmosphere of dry nitrogen. The septa-sealed tubes

were removed from the glovebag and massed. Approximately 20 mL of hexane and the requisite volume of stock solution of the second adsorbate were then added to the zeolite composite and incorporation of the second adsorbate was carried out as described above.

During the incorporation of the precursors into the zeolite framework, the utmost care was taken to keep the zeolite sample dry. In particular, manipulation of the dried samples was carried out in an atmosphere of nitrogen, and the samples were maintained in sealed vessels in order to avoid uptake of water during periods of stirring and centrifuging. The concentration of each reagent within the NaY samples was determined by UV analysis of the decants and is reported as the loading level in molecules per cavity, or the average fractional occupancy, $\langle S \rangle$.

Time-Resolved Diffuse Reflectance. Time-resolved diffuse reflectance experiments were carried out using a nanosecond laser photolysis system. The excitation source was a Lambda-Physik excimer laser containing a Xe/HCl/He gas mixture (308 nm, < 100 mJ, < 10 ns/pulse). Time-resolved optical spectroscopy was used to monitor the photogenerated transients. The detection system consists of a pulsed 75 W xenon-arc lamp, a monochromator, and a photomultiplier tube, which is used to monitor changes diffuse reflectance. Diffuse reflectance experiments involve measuring the fraction of reflected light absorbed by the transient, denoted as the reflectance change, $\Delta J/J_o$, where J_o is the reflectance intensity before laser excitation and ΔJ is the change in reflectance intensity after excitation due to absorption by photogenerated transients. The reflected light is focused through a grating monochromator into a photomultiplier system before being captured with a Tektronix 620A digitizing oscilloscope and transferred via a GPIB interface to a Power Macintosh 7100 computer that controls the laser system using a program written with LabView 3.0 software. The resulting apparatus permits the study of reactive intermediates with lifetimes $\geq$20 ns. Zeolite samples were contained in quartz cells constructed with 3×7 mm^2 tubing and were either evacuated under reduced pressure (10^{-4} Torr) and permanently sealed or purged with dry nitrogen, oxygen, or nitrous oxide for 30−60 min prior to laser photolysis. The sample cell was moved and/or shaken throughout the laser experiment to ensure that a fresh region of the zeolite surface was examined with each laser shot.

Acknowledgment. This work was supported by the Natural Sciences and Engineering Research Council of Canada (NSERC). We thank NSERC for supporting our research program.

Supporting Information Available: Data describing intracavity and intermolecular distances in NaY, and the distributions of DMB and DCB as a function of occupancy levels are given in Tables 1S to 3S. This material is available free of charge via the Internet at http://pubs.acs.org.

References and Notes

(1) Turro, N. J. *Acc. Chem. Res.* **2000**, *33*, 637−646.
(2) Ramamurthy, V.; Robbins, R. J.; Thomas, K. J.; Lakshminarasimhan, P. H. *Organized Molecular Assemblies in the Solid State*; Whitesell, J. K., Ed.; John Wiley & Sons Ltd.: New York, 1999; pp 63−140.
(3) Ramamurthy, V. *Photoprocesses of Organic Molecules Included in Zeolites*; Ramamurthy, V., Ed.; VCH: New York, 1991; pp 429−493.
(4) Dutta, P. K. *J. Inclusion Phenom. Mol. Recognit. Chem.* **1995**, *21*, 215−237.
(5) Thomas, J. K. *Chem. Rev.* **1993**, *93*, 301−320.
(6) Yoon, K. B. *Chem. Rev.* **1993**, *93*, 321−339.
(7) Breck, D. W. *Zeolite Molecular Sieves: Structure, Chemistry and Use*; John Wiley and Sons: New York, 1974.
(8) Rabo, J. A. *Zeolite Chemistry and Catalysis*; ACS Monograph No. 171; American Chemical Society: Washington, DC, 1976.
(9) Dyer, A. *An Introduction to Zeolite Molecular Sieves*; John Wiley and Sons: Bath, 1988.
(10) van Bekkum, H.; Flanigen, E. M.; Jansen, J. C. *Introduction to Zeolite Science and Practice*; Elsevier Science Ltd.: Amsterdam, 1991.
(11) Mumpton, F. A. *Proc. Natl. Acad. Sci. U.S.A.* **1999**, *96*, 3463−3470.
(12) Sherman, J. D. *Proc. Natl. Acad. Sci. U.S.A.* **1999**, *96*, 3471−3478.
(13) Hölderich, W.; Hesse, M.; Näumann, F. *Angew. Chem., Int. Ed. Engl.* **1988**, *27*, 226−246.
(14) Alvaro, M.; García, H.; García, S.; Marquez, F.; Scaiano, J. C. *J. Phys. Chem. B.* **1997**, *101*, 3043−3051.
(15) Corma, A. *Chem. Rev.* **1995**, *95*, 559−614.
(16) Baldovi, M. V.; Cozens, F. L.; Fornes, V.; García, H.; Scaiano, J. C. *Chem. Mater.* **1996**, *8*, 152−160.
(17) Cozens, F. L.; Regimbald, M.; García, H.; Scaiano, J. C. *J. Phys. Chem.* **1996**, *100*, 18165−18172.
(18) Cozens, F. L.; Cano, M. L.; García, H.; Schepp, N. P. *J. Am. Chem. Soc.* **1998**, *120*, 5667−5673.
(19) Ramamurthy, V.; Lakshminarasimhan, P.; Grey, C. P.; Johnston, L. J. *Chem. Commun.* **1998**, 2411−2424.
(20) Bracaleon, L.; Brousmiche, D.; Rao, V. J.; Johnston, L. J.; Ramamurthy, V. *J. Am. Chem. Soc.* **1998**, *120*, 4926−4933.
(21) Ramamurthy, V. *J. Am. Chem. Soc.* **1994**, *116*, 1345−1351.
(22) Turro, N. J.; Lei, X.; Li, W.; McDermott, A.; Abrams, L.; Ottavianai, M. F.; Beard, H. S. *Chem. Commun.* **1998**, 695−696.
(23) Turro, N. J.; McDermott, A.; Lei, X.; Li, W.; Abrams, L.; Ottavianai, M. F.; Beard, H. S.; Houk, K. N.; Beno, B. R.; Lee, P. S. *Chem. Commun.* **1998**, 697−698.
(24) Choi, S. Y.; Park, Y. S.; Hong, S. B.; Yoon, K. B. *J. Am. Chem. Soc.* **1996**, *118*, 9377−9386.
(25) Yoon, K. B.; Park, Y. S.; Kochi, J. K. *J. Am. Chem. Soc.* **1996**, *116*, 12710−12718.
(26) Yoon, K. B.; Hubig, S. M.; Kochi, J. K. *J. Phys. Chem.* **1994**, *98*, 3865−3871.
(27) Sankararaman, S.; Yoon, K. B.; Yabe, T.; Kochi, J. K. *J. Am. Chem. Soc.* **1991**, *113*, 1419−1421.
(28) Liu, X.; Iu, K.; Thomas, J. K. *J. Phys. Chem.* **1994**, *98*, 7877−7884.
(29) Ledney, M.; Dutta, P. K. *J. Am. Chem. Soc.* **1995**, *117*, 7687−7695.
(30) Hashimoto, S. *J. Chem. Soc., Faraday Trans.* **1997**, *93*, 4401−4408.
(31) Jortner, J.; Bixon, M. *Electron Transfer: from isolated molecules to biomolecules*; J. Wiley: New York, 1999; Vol. 106−107.
(32) Sunström, V. *Femtochemistry and Femtobiology*; Imperial College Press: London, 1996.
(33) Mariano, P. S. *Advances in Electron Transfer Chemistry*; Jai Press: Greenwich, CT, 1991−1994; Vol. 1−4.
(34) Kalyanasundaram, K. *Photochemistry in Microheterogeneous Systems*; Academic Press: New York, 1987.
(35) Fox, M. A. *Top. Curr. Chem.* **1991**, *159*, 68−101.
(36) Whitten, D. G. *Acc. Chem. Res.* **1980**, *13*, 83−90.
(37) Gust, D.; Moore, T. A.; Moore, A. L. *Z. Phys. Chem.* **1999**, *213*, 149−155.
(38) Kuciauskas, D.; Liddell, P. A.; Lin, S.; Stone, S. G.; Moore, A. L.; Moore, T. A.; Gust, D. *J. Phys. Chem. B* **2000**, *104*, 4307−4321.
(39) Dutta, P. K.; Ledney, M. *Prog. Inorg. Chem.* **1996**, *44*, 209−271.
(40) Joachim, C.; Roth, S. *Atomic and Molecular Wires*; ACS Monograph No. 341; Kluwer: Dordrecht, 1997.
(41) Leatherman, G.; Durantini, E. N.; Gust, D.; Moore, T. A.; Moore, A. L.; Stone, S.; Zhou, Z.; Rez, P.; Liu, Y. Z.; Lindsay, S. M. *J. Phys. Chem. B* **1999**, *103*, 4006−4010.
(42) Dutta, P. K.; Incavo, J. A. *J. Phys. Chem.* **1987**, *91*, 4443−4446.
(43) Dutta, P. K.; Turberville, W. *J. Phys. Chem.* **1992**, *96*, 9410−9416.
(44) Borja, M.; Dutta, P. K. *Nature* **1993**, *362*, 43−45.
(45) Vitale, M.; Castagnola, N. B.; Ortins, N. J.; Brooke, J. A.; Vaidyalingam, A.; Dutta, P. K. *J. Phys. Chem. B* **1999**, *103*, 2408−2416.
(46) Persaud, L.; Bard, A. J.; Campion, A.; Fox, M. A.; Mallouk, T. E.; Webber, S. E.; White, J. M. *J. Am. Chem. Soc.* **1987**, *109*, 7309−7314.
(47) Krueger, J. S.; Mayer, J. E.; Mallouk, T. E. *J. Am. Chem. Soc.* **1988**, *110*, 8232−8234.
(48) Kim, Y. L.; Mallouk, T. E. *J. Phys. Chem.* **1992**, *96*, 2879−2885.
(49) Brigham, E. S.; Snowden, P. T.; Kim, Y.; Mallouk, T. E. *J. Phys. Chem.* **1993**, *97*, 8650−8655.
(50) Yonemoto, E. H.; Kim, Y.; Schmehl, R. H.; Wallin, J. O.; Shoulders, B. A.; Richardson, B. R.; Haw, J. F.; Mallouk, T. E. *J. Am. Chem. Soc.* **1994**, *116*, 10557−10563.
(51) Sykora, M.; Kincaid, J. R. *Nature* **1997**, *387*, 162−164.
(52) Corma, A.; Fornés, V.; García, H.; Miranda, M.; Primo, J.; Sabater, M. *J. Am. Chem. Soc.* **1994**, *116*, 2276−2280.

(53) Corma, A.; Fornés, V.; García, H.; Miranda, M.; Sabater, M. *J. Am. Chem. Soc.* **1994**, *116*, 9767−9768.
(54) Fornés, V.; García, H.; Miranda, M. A.; Mojarrad, F.; Sabater, M.; Suliman, N. N. E. *Tetrahedron* **1996**, *57*, 7750−7760.
(55) Sanjuan, A.; Mercedes, A.; Aguirre, G.; García, H.; Scaiano, J. C. *J. Am. Chem. Soc.* **1998**, *120*, 7351−7352.
(56) Li, X.; Ramamurthy, V. *Tetrahedron Lett.* **1996**, *37*, 5235−5238.
(57) Hashimoto, S.; Hagiwara, N.; Asahi, T.; Masuhara, H. *Langmuir* **1999**, *15*, 3123−3133.
(58) Liu, X.; Iu, K.-K.; Thomas, J. K. *J. Phys. Chem.* **1989**, *93*, 4120−4128.
(59) Iu, K.-K.; Thomas, J. K. *Langmuir* **1990**, *6*, 471−478.
(60) Kemp, D. R.; Porter, G. *Chem. Commun.* **1969**, 1029−1030.
(61) Kawai, K.; Shirota, Y.; Tsubomura, H.; Mikawa, H. *Bull. Chem. Soc. Jpn.* **1972**, *45*, 77−81.
(62) Gschwind, R.; Haselbach, E. *Helv. Chim. Acta* **1979**, *62*, 941−955.
(63) Andre, J. J.; Weill, G. *Mol. Phys.* **1968**, *15*, 97−99.
(64) Hubig, S. M.; Bockman, T. M.; Kochi, J. K. *J. Am. Chem. Soc.* **1997**, *119*, 2926−2955.
(65) Scaiano, J. C.; de Lucas, N. C.; Andraos, J.; García, H. *Chem. Phys. Lett.* **1995**, *223*, 5−9.
(66) Scaiano, J. C.; Kaila, M.; Sonia, C. *J. Phys. Chem. B* **1997**, *101*, 8564−8568.
(67) Cozens, F. L.; O'Neill, M.; Schepp, N. *J. Am. Chem. Soc.* **1997**, *119*, 7583−7584.
(68) O'Neill, M. A.; Cozens, F. L.; Schepp, N. P. *J. Am. Chem. Soc.* **2000**, *122*, 6017−6027.
(69) Maslak, P.; Chapman, W. H., Jr. *J. Org. Chem.* **1996**, *61*, 2647−2656.
(70) (a) It has previously been demonstrated that detectable quantities of radical ion pairs can be observed upon irradiation of existing charge-transfer complexes in zeolites. (b) ref 26.
(71) Schepp, N. P.; Johnston, L. J. *J. Am. Chem. Soc.* **1996**, *118*, 2872−2881.
(72) Shida, T. *Electronic Absorption Spectra of Radical Ions*; Elsevier: Amsterdam, 1988.
(73) Cozens, F. L.; Bogdanov, R.; Regimbald, M.; García, H.; Marti, V.; Scaiano, J. C. *J. Phys. Chem. B* **1997**, *101*, 6821−6829.
(74) Iu, K.-K.; Thomas, J. K. *J. Phys. Chem.* **1991**, *95*, 506−509.
(75) Iu, K.-K.; Thomas, J. K. *Colloids Surf.* **1992**, *63*, 39−48.
(76) Liu, X.; Iu, K.-K.; Thomas, J. K. *Chem. Phys. Lett.* **1993**, *204*, 163−167.
(77) Iu, K.-K.; Liu, X.; Thomas, J. K. *J. Photochem. Photobiol. A* **1994**, *79*, 103−107.
(78) Lednev, I. K.; Mathivanan, N.; Johnston, L. J. *J. Phys. Chem.* **1994**, *98*, 11444−11451.
(79) Hashimoto, S.; Mutoh, T.; Fukumura, H.; Masuhara, H. *J. Chem. Soc., Faraday Trans.* **1996**, *92*, 3653−3660.
(80) Zhang, G.; Liu, X.; Thomas, J. K. *Radiat. Phys. Chem.* **1998**, *51*, 135−152.
(81) Liu, X.; Zhang, G.; Thomas, J. K. *J. Phys. Chem.* **1995**, *99*, 10024−10034.
(82) Liu, X.; Zhang, G.; Thomas, J. K. *J. Phys. Chem. B* **1997**, *101*, 2182−2194.
(83) Nakazato, C.; Masuda, T. *Bull. Chem. Soc. Jpn.* **1986**, *59*, 2237−2239.
(84) Masuhara, H.; Saito, T.; Maeda, Y.; Mataga, N. *J. Mol. Struct.* **1978**, *47*, 243−259.
(85) Samoilova, R. I.; Shublin, A. A.; Bowman, M. K.; Hüttermann, J.; Dikanov, S. A. *Chem. Phys. Lett.* **2000**, *316*, 404−410.
(86) Perrin, M. J. *C. R. Acad. Sci.* **1923**, *177*, 469−475.
(87) Perrin, M. F. *C. R. Acad. Sci.* **1924**, *178*, 1978−1980.
(88) Turro, N. J. *Modern Molecular Photochemistry*; Benjamin-Cummings: Menlo Park, CA, 1978.
(89) Turberville, W.; Robins, D. S.; Dutta, P. K. *J. Phys. Chem.* **1992**, *96*, 5024−5029.
(90) An estimate of Y_∞ may be obtained from the experimental data if sufficiently high concentrations of quencher are used. However, it can also be extrapolated by fitting a plot of $(Y/Y_\infty) - 1$ versus [Q] to an exponential and adjusting Y_∞ such that the exponential has a coefficient of 1.
(91) The yield of carbocation absorbing at 360 nm was corrected for absorption at this wavelength by the Chl radical anion (ϵ 450 nm = 9700, ϵ 360 nm = 3120), and the chloranil triplet (ϵ 500 nm = 7200, ϵ 450 nm = 3600, ϵ 360 nm = 6480).
(92) Molecular radii of 3.2 Å for Chl; 7.5 Å for DMB.; 5 Å for An; and 4.1 Å for DCB were determined from one-half of the longest interatomic distances estimated from a molecular model constructed with standard bond lengths and bond angles.
(93) Sykora, M.; Kincaid, J. R.; Dutta, P. K.; Castagnola, N. B. *J. Phys. Chem. B* **1999**, *103*, 309−320.
(94) Maslak, P.; Chapman, W. H., Jr. *J. Org. Chem.* **1990**, *55*, 6334−6347.